Simulation of multi-polarisation LightSAR imagery from AIRSAR

Stephen McNeill and David Pairman

Landcare Research
PO Box 69 Lincoln 8152, New Zealand
mcneills@landcare.cri.nz, pairmand@landcare.cri.nz

Abstract

The methodology used to simulate both dual and quad-polarisation L-band images from NASA's planned LightSAR is described. In choosing the methodology, the along track tilt-induced shift in orientation angle of the polarisation signature observed by Schuler et al (1996) was investigated. Clear evidence of this phenomenon was observed for P and L bands but the opposite effect was seen in C-band. The synthesised LightSAR imagery has been visually assessed and it appears that dual polarisation 4-look imagery will be the most suitable mode for forest inventory work.

Keywords: *AIRSAR, polarimetric SAR, LightSAR*

1 Introduction

As part of the 1996 AIRSAR campaign, a variety of test sites were flown in New Zealand. The focus for Landcare Research, using this data, has been the estimation of biomass from radar data. Although our primary interest is with native vegetation, part of the study has involved plantation forestry. Now interest from the forestry industry is emerging as one of the strongest areas, both to use radar techniques operationally in the future, and also to become involved in any future AIRSAR mission. This industry interest is not only for biomass, but, more importantly, in radar based techniques for routinely updating forest inventory information. Radar has the advantage of weather independence and thus is suited to regular surveys where the timing of image acquisition is critical.

Unfortunately our research to date using Radarsat-1 single polarisation (HH) C-band data has not provided consistent results that clearly differentiate the targets of interest. However, our experience with full polarisation AIRSAR data shows that there is significant information in the polarisation characteristics to assist such inventory approaches [Pairman *et al*, 1999]. We also feel, based on our work with JERS-1 data, that L-band data is much better suited to the type of classification required for forest inventory [North and Wu, 1999]. With the lack of any current operational civil L-band satellite and because of the potential of polarisation, it is important to look forward to future satellites and what they may be capable of delivering for forest inventory applications.

The most promising planned satellite for forest inventory applications appears to be NASA's LightSAR, with a planned launch date near the end of 2002 [Potts, 1998]. This instrument is still very much at the concept stage. It is based on a dual/quad polarisation L-band SAR instrument, but may well have an additional C-band capability. The imaging characteristics are flexible with a variety of resolution / swath width / polarisation modes. We have chosen to simulate the 25 m resolution quad and dual polarisation modes as these appear best suited to the application.

In the next section, the overall scheme for simulating the LightSAR imagery is detailed. One component of this process is the potential adjustment of the polarisation signature before extracting the specific points provided by LightSAR. An along track tilt-related shift in the orientation angle of the polarisation signature has been noted by Schuler et al (1996). In section 3, we investigate both this phenomenon and also another potential formulation of the relationship. Results of the LightSAR simulations are presented in section 4 along with a summary and conclusions.

2 LightSAR simulation procedure

In order to simulate LightSAR, or indeed any future platform, it is necessary to make modifications to the AIRSAR data so that the target characteristics are correctly represented in the new simulated sensor. Implicit in this process is the assumption that there are sufficient degrees of freedom in the AIRSAR data to represent the restricted nature of the simulated data set. Although this is certainly true for the LightSAR modes of primary interest to the authors (dual and quad-polarisation modes) it is not the case for the planned high spatial resolution modes. In this latter case, an alternative surrogate data set needs to be found.

In the event that the AIRSAR data is satisfactory, several corrections are required for a first-order simulation. First, the spatial resolution of the data must be reduced to meet the nominal values specified by the new sensor. Second, the polarisation response of the target must be modified to account for the difference between the viewing conditions of the simulated sensor and AIRSAR. Third, an appropriate noise model needs to be applied to the data to meet the expected number of looks. Each of these corrections will be dealt with, in turn.

Some of the steps involving a digital elevation model are more conveniently carried out in the map domain rather than in the image domain. Rather than attempting to simulate a slant range LightSAR image, we will simulate a derived image, complete with corrections that we would normally use for such imagery. This includes ortho-rectification allowing simplifications by avoiding projecting information back into the slant range domain.

2.1 Spatial resolution

From table 1 it can be seen that the AirSAR data has a different resolution in the azimuth and range directions. Furthermore, both dimensions are oversampled by a significant margin.

	L-band	C-band	P-band
Nominal slant range resolution	5.5	5.5	5.5
Nominal azimuth resolution	27.0	21.6	63.0
Slant range pixel spacing	3.33	3.33	3.33
Azimuth range pixel spacing	9.26	9.26	9.26

Table 1 AirSAR resolution characteristics.

The resolution indicated for the LightSAR modes of interest is 25 m. However we assume that this is intended to be an eventual ground range figure and that the slant range will be closer to 17 m (25 m ground range corresponds to 17.6 m slant range for a 45 ° look angle). The AirSAR azimuth resolution is already slightly poorer than the LightSAR figure, however the slant range resolution needs to be reduced to ~17 m. In image space 17 m, equates to 5.2 pixels. We therefore approximate the required spatial filter using a simple 1x5 pixel low pass window filter.

2.2 Ortho-rectification

Before any spatial measurements can be extracted or comparisons / combinations with other data made, remotely sensed imagery first needs to be re-sampled to a common grid, usually based on a standard mapping projection. In the New Zealand case this is normally the NZ metric map grid (NZMG), and we routinely ortho-rectify both optical and radar imagery to this base. For radar imagery this is particularly important due to the exaggerated foreshortening and layover effects of terrain.

A flat earth model is sufficient for AirSAR imagery, where a digital elevation model is used with a geometric model to calculate the slant range position where each ground range pixel should be sampled from. Ground control points

are used to anchor the geometric model onto the mapping projection.

For the LightSAR simulation, reduced resolution AirSAR imagery was re-sampled onto a 25 m posting ground range projection in the NZMG. The digital elevation model used was generated by interpolation of 20 m contour data.

2.3 Sigma-nought surface area correction

For uniform ground cover, backscattered power varies in proportion to the area of distributed scatterers contributing to each pixel. This causes slopes facing to radar instrument to appear brighter than those facing away. Provided layover is not occurring, a correction for this phenomena can be calculated from the surface geometry. Correcting imagery to the sigma-nought for a flat surface equivalent improves the ability of classifiers to use power or amplitude as a metric. For AirSAR this correction is particularly important, as there is a large difference in the level terrain incidence angle from one edge of the scene to the other (22-63°).

The correction is based on the surface area passing through a tube aligned orthogonally to both the slant range vector and the azimuth (flight) direction (Pairman *et al*, 1997). Thus, radar cross section, $\sigma_{0,}$ generated by:

$$\sigma_0 = \beta_0.\cos(\omega)$$
$$\omega = \arccos[\cos\gamma_z \sin\theta_i - \sin\gamma_z \cos\theta_i \cos(\Delta az)]$$

where γ_z is the local slope, θ_i the local (flat surface) incidence angle at a given point, and Δaz is the difference between the azimuth to the satellite and the azimuth of the surface normal. This correction is most conveniently applied in the map domain where the surface parameters are available from a digital elevation model. The look angle, θ_i can easily be derived in this domain by ortho-rectifying an image of slant range and using the knowledge of aircraft height.

2.4 Polarisation signature adjustment

At this stage, the polarisation signature can also be adjusted to a level surface equivalent, provided the full signature is available. This process is covered in detail in section 3.

2.5 Noise adjustment.

One of the most significant factors effecting the usefulness of radar data is the speckle noise content. At this stage we make the assumption that we have a noise free estimate of the radar cross section. Although not perfect, the original AirSAR data is 18 look and has been further smoothed by filtering with a 5x1 pixel filter. The correct simulation of multi-look SAR data is difficult due to both correlation between pixels and correlation between looks (Rignot & Chellappa, 1991). We take a simplistic approach based on Rignot & Chellappa, 1991, by assuming independent pixels and looks. Each look is synthesised using the radar cross section as the mean of a negative exponential random distribution:

$$p(|a^2|/<i>) = \frac{1}{<I>}\exp(-\frac{|a|^2}{<I>})$$

where a is the complex amplitude and $<I>$ is the mean intensity of the pixel. The N independent looks are then summed to produce the multi-look amplitude.

3 Polarisation correction

The AIRSAR sensor illuminates the target nominally from 22 to 63 degrees local incidence angle from near- to far-

range, respectively. For a satellite sensor, the variation of local incidence angle, neglecting the local topography for the moment, varies over a much smaller range, perhaps as little as a few degrees around a nominal value of, for example, 38 degrees. In this section we investigate if the difference between the simulated sensor incidence angle and the AIRSAR incidence angle causes a change in the polarisation response which must be corrected. In order to make a correction, the AIRSAR full polarisation response is required, as well as a model that relates a change in the local incidence angle, including the local topography, to a change in the polarisation response.

The polarisation response for a given target can be obtained through the polarisation synthesis equation, expressed in terms of the modified Stokes scattering operator, here termed M, in the following form (van Zyl & Ulaby 1990):

$$\sigma(\phi_r, \chi_r, \phi_t, \chi_t) = \frac{4\pi}{k^2} v^T M v$$

with χ the ellipticity, ϕ the orientation, and k the appropriate wavenumber. Frequently, the above equation is simplified for diagrammatic reasons by selecting the case when $\phi_r = \phi_t$ and $\chi_r = \chi_t$, giving the co-polarisation response, or $\phi_r = \phi_t + \pi/2$ and $\chi_r = \chi_t + \pi/2$, giving the cross polarisation response. The values of the quad-polarisation data set can be visualised as points on the co- and cross-polarisation surfaces at appropriate values of χ and ϕ. Thus, assuming that an appropriate model can be found for the polarisation response for a given local incidence angle, the values of the simulated sensor can be retrieved

A polarisation correction model, and verification

One such correction model has been suggested [Schuler *et al.* 1996] from studies concerning the polarisation effects of long-wave tilts on the ocean surface. These studies suggested that the co-polarisation response of a tilted land surface would be shifted in the orientation axis by an amount equal to the resolved component of the azimuthal tilt (*stilt*), while the response would be invariant in the ellipticity axis. The authors used this relationship to estimate azimuthal components of slope, which, suitably integrated, gave estimates of the topography. Further, the authors suggested that the principal cause of the observed shift was in one of the cross-terms of the covariance matrix (calculable from the Stokes matrix values) of c_{hhhv}, and therefore concluded from related symmetry studies [Yuen *et al.* 1994] that the linear relationship between the orientation shift and the azimuthal tilt would be observed when the resolved tilt was sufficient to modulate the symmetry properties of the target. This latter observation is important, since it relies on the assumption that the size and distribution of the scatterers within the target are sufficiently large with respect to the wavelength to induce an effect in the relevant covariance matrix element (see below). Although [Schuler *et al.* 1996] do not consider the cross-polarisation response, the implication is that a similar effect also occurs in that case.

Following the symmetry arguments used by Schuler *et al.* we also investigated if the surface tilt component in the azimuth direction with respect to the viewing vector (*vtilt*) would not be a more closely related to the observed shift in the polarisation signature. Unlike *stilt*, the *vtilt* angle does vary across the scene as the look angle changes.

In the present AIRSAR case of simulating LightSAR data, the model suggested by [Schuler *et al.* 1996] would be used in the reverse sense. That is, given a resolved azimuthal tilt from a known digital elevation model, as well as the look-angle conditions for the AIRSAR and LightSAR cases, the polarisation surface is shifted (using the model) in the orientation direction, then the LightSAR quad-polarisation elements extracted.

Analytically, the surface tilt can be expressed in terms of the imaging parameters as follows. First, it is assumed that the aircraft travels at a heading θ_h clockwise with respect to north, with the local incidence angle θ_i at a given point. Assuming a flat earth model, which is sufficient for the AIRSAR case, the local incidence angle can be given by:

$$\theta_i = arcos((H-h)/s)$$

with H and h the aircraft and terrain height, respectively, and s the slant range. Assuming the AIRSAR scene is rectified to a Cartesian map system, the AIRSAR unit look angle vector, or equivalently the incidence angle vector, is then given by $\boldsymbol{p} = [-\cos\theta_h.\sin\theta_i \;\; \sin\theta_h.\sin\theta_i \;\; \cos\theta_i]^T$. A second vector can be derived from $\boldsymbol{p}$ in the along-track direction, but in the Cartesian plane, defined by $\boldsymbol{q} = [\sin\theta_h \;\; \cos\theta_h \;\; 0]^T$, which, with the z-component of the surface normal $\boldsymbol{N}$ gives the along-track component of the surface tilt *stilt:*

$$stilt = \arctan\left(\frac{\boldsymbol{N}.\boldsymbol{q}}{\boldsymbol{N}.\boldsymbol{z}}\right)$$
$$= \arctan\left(\frac{N_x \sin\theta_h + N_y \cos\theta_h}{N_z}\right)$$

Typically, the components of the surface normal will be expressed in terms of the slope and azimuth, derived from some digital elevation model by a suitable approximation to the derivative. There are several representations of the slope and aspect, and for numerical convenience we choose to use the zenith slope (the complement of the slope) γ_z and the azimuth γ_a, measured in the same sense as the aircraft heading. In this case, the unit surface normal is expressed as $\boldsymbol{N} = (\sin\gamma_a.\sin\gamma_z \;\; \cos\gamma_a.\sin\gamma_z \;\; \cos\gamma_z)^T$, in which case the expression for *stilt* simply reduces to:

$$stilt = \arctan(\tan\gamma_z.\cos(\gamma_a - \theta_h))$$

Thus, a calculation of the elevation model slope and azimuth, and the aircraft heading, according to the polarisation-shift model, immediately gives the correction angle *stilt*. A similar derivation can be done to generate azimuth component of surface tilt with respect to the plane through the viewing vector and flight vector:

$$vtilt = \arctan\left(\tan\gamma_z.\frac{\cos(\gamma_a - \theta_h)}{\cos\theta_i}\right)$$

However, the correctness of Schuler *et al.'s* approach or our alternative had to be verified for the scatterers within the New Zealand AIRSAR scene. To do this, two separate targets were chosen within scene CM5231. The first was a uniform *Pinus radiata* stand, and the second was a region of mountain grass (tussock, or *Chionochloa*). For each target, samples from the averaged Stokes matrix were extracted and the co-polarisation surface formed for P-, L- and C-band. This surface was then correlated against the characteristic co-polarisation surface of the target, formed from the average Stokes matrix values of the ensemble of test points. The correlation was measured as a shift in orientation and ellipticity, with graphs of one such target (tussock) shown in figure 1.

A number of important conclusions can be drawn from figure 1 and the test statistics. First, all correlations are significant at the 1% level. This, in conjunction with the low R-values of the ellipticity plots, would suggest that there is a weak ellipticity dependence on the surface tilt, although it should be noted that the slope of the dependence at L-band is many times less than the orientation dependence. Second, for the number of sample points, only the L-band satisfies the null hypothesis that the slope of the orientation-versus-gamma is unity, at the 1% level of significance, although the P-band case would be significant at a slightly lower level of significance. Third, and unexpectedly, the strong correlation value of the orientation-versus-gamma graph in C-band indicates an *anti*-correlation between the two quantities. In fact, the C-band case has a t-statistic, for a slope of -1, of 0.55, quite significant at the 1% level. Similar results also apply for the *Pinus radiata* case.

A similar analysis using the *vtilt* angle produced almost identical results. However the R-values were slightly lower

suggesting that the mechanism is independent of the look angle.

Collectively, these results suggest that the simple model of [Schuler *et al.* 1996] is satisfied for the L-band case, although there is a suggestion of a weak, low-slope relationship between surface tilt and ellipticity shift. The observed anti-correlation in the C-band case is unusual, and warrants further study. The conclusion from this experiment is that the Schuler model provides a reasonable account of the shifts that are required to transform AIRSAR data to a common flat surface representation, even if the weak ellipticity dependence is ignored. Unfortunately, as only component (hh, hv and vv) values would be available from LightSAR, it would not be possible to similarly adjust LightSAR data to a flat surface polarisation representation.

4 Simulation results and summary

Figure 2 shows the original AirSAR L-band HH component along with the reduced resolution four- and two-look simulated LightSAR versions appropriate for dual and quad polarisation modes from that instrument. It is apparent from figure 2 that the effective resolution is becoming seriously degraded in the 2-look quad polarisation imagery. The dual polarisation LightSAR modes provide either HH & HV or VV & HV, while the quad polarisation mode provides HH, HV, VV, VH. However as HV and VH should be identical, there is limited gain in moving to quad polarisation at the expense of halving the number of looks. At least visually, the like polarisation images (HH and VV) appear quite similar while the cross polarisation (HV) image appears quite different. This indicates that most of the information content will be contained in a dual polarisation HH, HV or VV, HV combination.

This paper has concentrated on the steps required to synthesise dual and quad polarisation LightSAR images from AirSAR data. As part of this study we have investigated the azimuth-tilt-induced shift in polarisation signature observed by other authors. This phenomenon, while present in L- and P-bands is not as clear as previously reported, perhaps due to non-homogeneity in the targets. We also observed a polarisation signature displacement in the opposite direction with C-band, for which we have no current explanation.

Detailed assessment of the synthesised LightSAR imagery requires further work involving a variety of classification techniques and a wider variety of imagery. However, our initial impression is that the dual polarisation 4-look data will be the most suitable mode for forest inventory work.

References

Potts, D., 1998, "LightSAR reference mission," Jet Propulsion Laboratory document *JPL-D-13946*, March 1998.

North, H.C. and Wu, Q.W., 1999, "Multiscale edge detection: a discussion on feature visibility," Proceedings *IEE Image Processing and its Applications Conference*, pp.547-551, Manchester, 12-15 July.

Pairman, D., Belliss, S.E. and McNeill, S.J., 1997, "Terrain influences on SAR backscatter around Mt Taranakim New Zealand," *IEEE Trans. Geoscience and Remote Sensing*, Vol. 35(4), pp 924-932.

Pairman, D., McNeill, S., Scott, N. and Belliss, S., 1999, "Vegetation identification and biomass estimation using AirSAR data," *Geocarto International*, Vol 14(3), pp 67-75.

Rignot, E. and Chellappa, R., 1991, "Segmentation of synthetic-aperture-radar complex data," *J. Opt. Soc. Am.*, Vol 8(9), pp 1499-1509.

Schuler, D.L., Lee, J-S., and De Grandi, G., 1996, "Measurement of topography using polarimetric SAR images," *IEEE Trans. Geoscience and Remote Sensing*, Vol. 34(5), pp 1266-1276.

van Zyl, J.J., and Ulaby, F.T., 1990, "Scattering matrix representation for simple targets," pp 17-52, in Ulaby, F.T., & Elachi, C. (eds) *Radar polarimetry for geoscience applications*, Artech House, Norwood, MA, 1990.

Yuen, S.H., Kwok, R., and Nghiem, S.V., 1994, “Polarimetric scattering and emission properties of targets with reflection symmetry,” *Radio Science*, Vol. 29(6), pp 1409-1420.

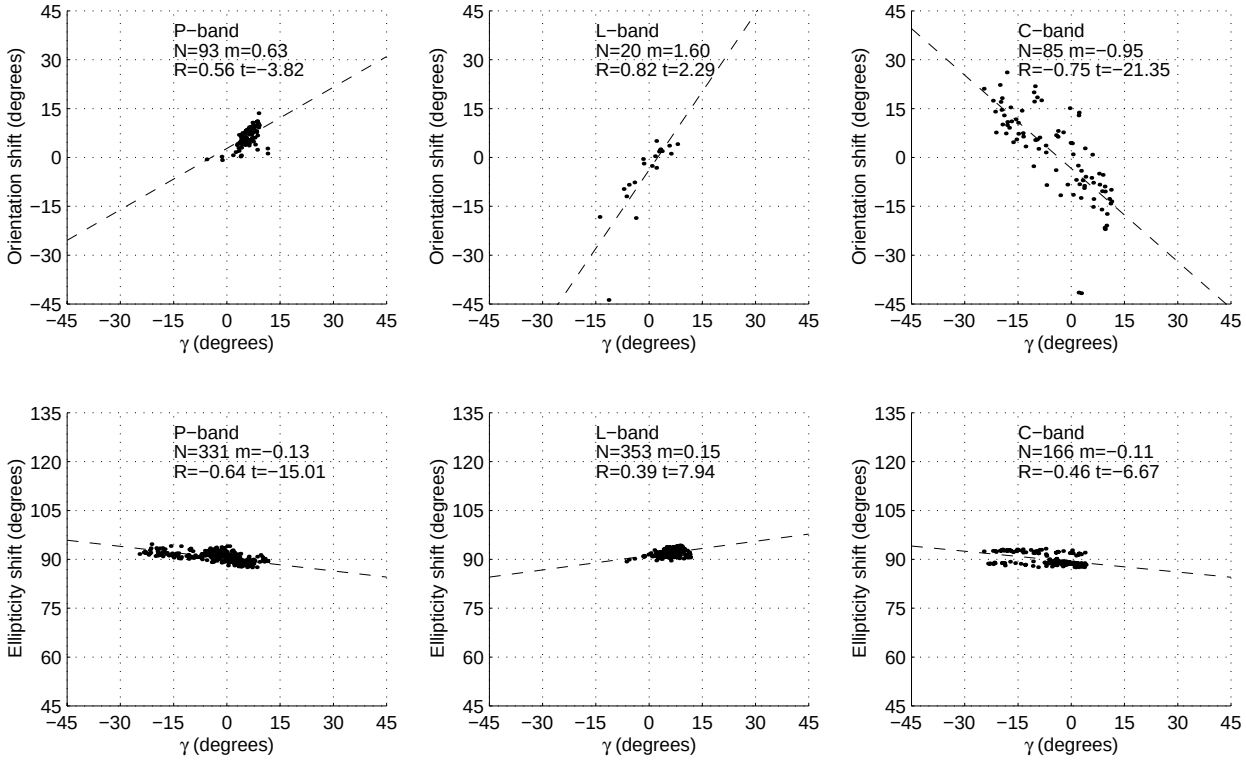

Figure 1 Orientation and ellipticity shift of a single target type (mountain grass or tussock) plotted against the along-track component of the surface tilt. The least-squares lines are drawn in each case, and the slope m, correlation coefficient R, and the number of test points N. The value of the t-statistic t has also been calculated, for the case of a slope of 1 in the upper graphs, and 0 in the lower set.

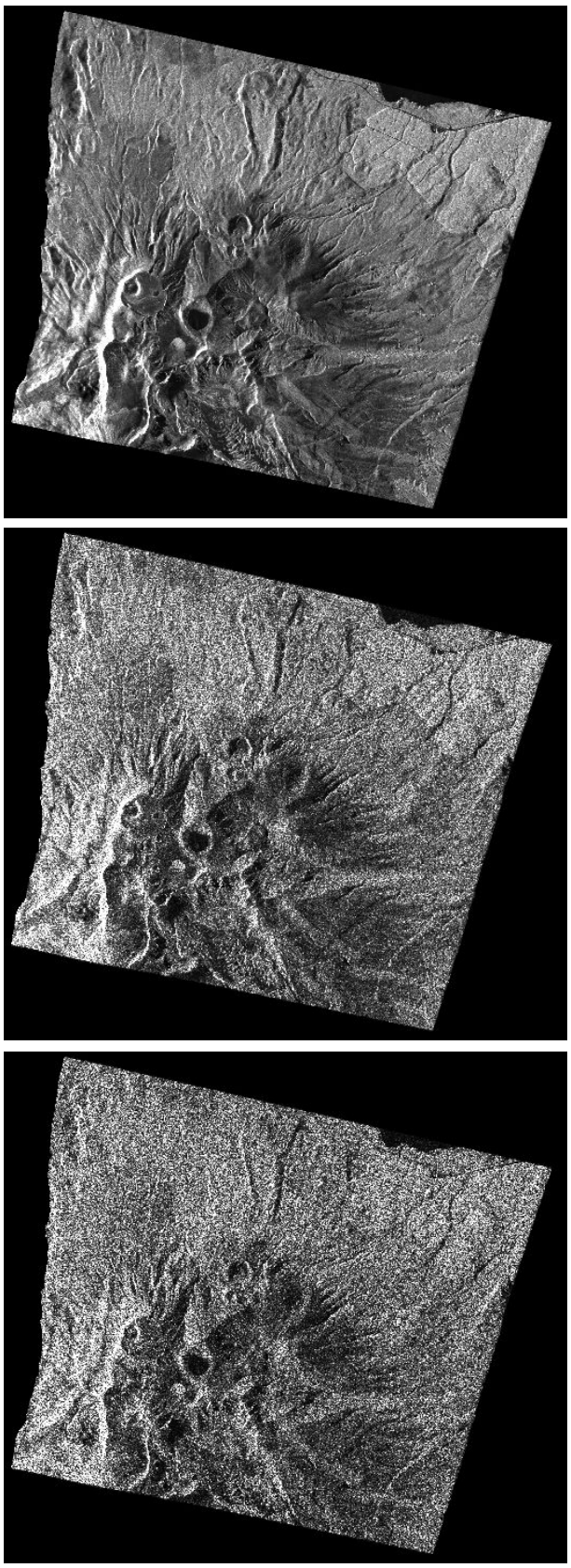

Figure 2 a) AirSAR L-band HH b) 4-look LightSAR HH c) 2-look LightSAR HH